ISSN 0915-633X

NATIONAL INSTITUTE FOR FUSION SCIENCE

The Meandering Orbit Effect on Stabilization of the Tilting Instability in a Field-Reversed Configuration

R. Horiuchi and T. Sato

(Received – Jan. 23, 1990)

NIFS-22 Mar. 1990

RESEARCH REPORT
NIFS Series

NAGOYA, JAPAN

THE MEANDERING ORBIT EFFECT ON STABILIZATION OF THE TILTING INSTABILITY IN A FIELD-REVERSED CONFIGURATION

Ritoku HORIUCHI

Science Project Corporation, Kuchita-Mimami 3-40-17-304

Asakita-Ku, Hiroshima 739-19, Japan

Tetsuya SATO

National Institute for Fusion Science,

Furocho, Chikusa-ku, Nagoya 464, Japan

Ion kinetic effect in the tilt disruption of a field-reversed configuration is investigated by means of a three-dimensional particle simulation. It is found that the tilt disruption is completely suppressed when $\bar{s} \approx 1$, where $\bar{s}$ measures the number of ion gyroradii over the radial distance between the magnetic separatrix line and the field-null line. Prolate magnetic well is formed around the field-null line, in which ions do not execute gyration but meander along the field-null line. For the case of $\bar{s} \approx 1$ a large number of ions exist in the magnetic well and move on stable orbits around the major axis with the average rotation velocity nearly equal to half of the thermal velocity. As $\bar{s}$ becomes larger than 1, the number of ions in the magnetic well decreases and the stabilization effect is reduced. It is also found that an anisotropy is created in the ion thermal pressure profile owing to the anisotropy of the meandering orbits and that the electric field fluctuation always remains at a low level, thus the electric field plays no essential role in the tilt stabilization.

Keywords field-reversed configuration, tilting instability, finite Larmor radius, ion kinetic stabilization, three-dimensional particle simulation, anisotropic thermal pressure, meandering orbit

I. Introduction

The field-reversed configuratin (FRC) is a compact toroidal device in which a high-beta plasma is confined by a simple magnetic geometry with a negligible toroidal magnetic field. The characteristic features, i.e., simple geometry and high-beta plasma, make the FRC attractive as a magnetic fusion device. However, it is pointed out that there exist two global instabilities leading to destruction of plasma confinement. One is the $n=2$ rotational instability where n is the toroidal mode number. This instability was found to be suppressed by applying the external multipole fields.[1] The other is the $n=1$ tilting instability.[2-4] However, no experimental evidence has so far been reported on the tilt disruption in the magnetohydrodynamic (MHD) time scale predicted by the linear analysis.[1,5] Two possibilities are conceivable to explain the discrepacy between the linear theory and the experiment. The first explanation is that the nonlinear saturation mechanism could protect the FRC plasma from the destructive growth of the tilt mode. Horiuchi and Sato[6] have carried out a three-dimensional full MHD simulation and found no evidence for the nonlinear saturation of the tilt mode except for a highly spinning case.

An alternative explanation may be given by taking into account the ion kinetic effect. That is, the stabilization effect due to the ion finite-Larmor radius (FLR) can operate effectively in the current devices since the device scale is comparable to the ion Larmor radius. Barnes et al.[7] derived the linear growth rate from a Vlasov-fluid dispersion equations and found that the tilt mode could be stabilized for a large gyroradius case of $\bar{s}\leq 2$, where $\bar{s}$ is defined by

$$\bar{s} = \int_{r_a}^{r_s} \frac{rdr}{r_s \lambda_i}, \tag{1}$$

r_s is the separatrix radius, r_a is the radius of the magnetic null, and λ_i is the local ion gyroradius. By using a two-fluid variation formalism Ishida el al.[8] have shown that a stabilization region would appear for a very highly prolate and small $\bar{s}$ case

due to the effect of the Hall term. Milroy et al.[9] have examined the ion kinetic effect by solving the nonlinear MHD equations including the Hall term. Their results indicate that the Hall term can reduce the growth rate of the tilt mode for the highly prolate and small $\bar{s}$ case. However, their analyses cannot fully explain the discrepacy between the theory and the experiment.[10] This is probably because the Hall term can represent only a part of the ion FLR effect. Particularly in the case where the field-null region exists the Hall term inclusion in the MHD equations is insufficient in dealing with the whole FLR effect.

One of the characteristic features of the FRC plasma is that a field-null line exists in the central plasma region due to the strong toroidal plasma current. For the device of $\bar{s} \approx 1$ most of the particles in the vicinity of field-null line cannot make gyration motions but reveal complex behaviors.[11] For reference, we show eight types of ion orbit in Fig. 1 for a one-dimensional model in which the magnetic field has only the z-component and its value depends only on the coordinate x in the form as $B_z(x) = B_0(x/x_0)$; x_0 is the scale height and B_0 is the characteristic value of the magnetic field. An ion is pushed in the negative y-direction with a velocity v_y from the initial point (x_0 , 0). For the case of the normalized Larmor radius $\lambda_i/x_0 = 0.22$ ions move along the gradient-B drift orbit. When $\lambda_i/x_0 > 0.25$, ions move across the field-null line and their orbits form a combined shape of two gradient-B drift orbits (figure-eight shape orbits). When the gyration velocity is larger than the critical one ($\lambda_i/x_0 > 0.303$), the ions drift to the direction opposite to that of the gradient-B drift. As the velocity (energy) increases further, ions execute meandering motions along a field-null line without any self-intersection of the orbit line ($\lambda_i/x_0 = 0.8$). In this way it is important to take into account the effect of the finite-sized particle-orbit in the real magnetic geometry on the global behavior of the FRC plasma.

The best way to investigate the FLR stabilization effect against the tilting instability is to carry out the macro-scale particle simulation that can describe both the

electron and ion FLR effects and the global behavior over the device scale simultaneously.[12,13] For this purpose we use a three-dimensional macro-scale particle simulation code in the cylindrical coordinates, which relies on the semi-implicit scheme. The initial condition and the simulation model are described in Sec. II. The results obtained from the particle simulation are discussed in comparison with the MHD result in Sec. III. The first half of Sec. III is devoted to discussions of the ion kinetic stabilization effect in connection with the character of the meandering orbit. We also discuss the anisotropy of the ion pressure profile, and the $\bar{s}$-dependence of the plasma rotation in the latter half of Sec. III. Finally we give a brief discussion on the electric field and the applicability of the model in Sec. IV.

II. Simulation model

It should be emphasized that not only ions but also electrons reveal fairly complex behaviors near the field-null point and the sharply curved edges of field lines in the FRC plasma. Thus, we must rely on a simualtion study that can adequately treat the nonlinear interaction between the electron thermal motion and the fluctuating field in the real geometry.

We study the FRC plasma in a cylindrical conducting vessel in which the plasma is confined by a uniform external field. The equations to be solved are the equations of motion

$$\frac{d(\gamma_j \mathbf{v}_j)}{dt} = \frac{q_j}{m_j}\left[\mathbf{E} + \frac{\mathbf{v}_j}{c}\times\mathbf{B}\right], \tag{2}$$

$$\frac{d\mathbf{x}_j}{dt} = \mathbf{v}_j, \tag{3}$$

and the Maxwell equations

$$\frac{1}{c}\frac{\partial \mathbf{B}}{\partial t} = -\nabla\times\mathbf{E}, \tag{4}$$

$$\frac{1}{c}\frac{\partial \mathbf{E}}{\partial t} = -\nabla\times\mathbf{B} - 4\pi\mathbf{j}, \tag{5}$$

$$\nabla\cdot\mathbf{B} = 0, \tag{6}$$

$$\nabla\cdot\mathbf{E} = 4\pi\rho, \tag{7}$$

where $\mathbf{x}_j(t)$,$\mathbf{v}_j(t)$ m_j and q_j are the position, the velocity, the rest mass and the charge of the j-th particle, and the relativistic γ-factor of the j-th particle is defined by

$$\gamma_j = 1/\sqrt{1-(\mathbf{v}_j\cdot\mathbf{v}_j)/c^2}. \tag{8}$$

The current density $\mathbf{j}(\mathbf{x},t)$ and the mass density $\rho(\mathbf{x},t)$ are obtained by summing over all the particles, namely,

$$\mathbf{j}(\mathbf{x},t) = \sum_{j=1}^{N} \frac{q_j\mathbf{v}_j(t)}{c}\,\delta(\mathbf{x}-\mathbf{x}_j(t)), \tag{9}$$

$$\rho(\mathbf{x},t) = \sum_{j=1}^{N} m_j\,\delta(\mathbf{x}-\mathbf{x}_j(t)), \tag{10}$$

where N is the total number of particles.

In principle we solve the evolutional equations (2)-(5) by assigning the initial conditions $\mathbf{x}_j(0)$, $\mathbf{v}_j(0)$, $\mathbf{B}(\mathbf{x},0)$ and $\mathbf{E}(\mathbf{x},0)$ which satisfy Eqs. (6), (7) and (10). In order to investigate the global stability of the FRC plasma, we consider a two-fluid MHD equilibrium as an initial model, which is described by

$$\frac{\partial P_i}{\partial r} = n_i q_i \frac{U_i}{c} B_z + m_i n_i \frac{U_i^2}{r}, \tag{11}$$

$$\frac{\partial P_i}{\partial z} = -\, n_i q_i \frac{U_i}{c} B_r, \tag{12}$$

$$\frac{\partial P_e}{\partial r} = n_e q_e \frac{U_e}{c} B_z, \tag{13}$$

$$\frac{\partial P_e}{\partial z} = -\, n_e q_e \frac{U_e}{c} B_r, \tag{14}$$

$$-\frac{\partial B_z}{\partial r} + \frac{\partial B_r}{\partial z} = -\,\frac{4\pi}{c}\,(\, n_i q_i U_i + n_e q_e U_e\,), \tag{15}$$

where the cylindrical coordinates (r,ϕ,z) are used, subscript i or e denotes ion or electron, $U_{i(e)}$ is the ϕ-component of the ion(electron) fluid velocity, $P_{i(e)}$ is the ion(electron) thermal pressure, and $n_{i(e)}$ is the ion(electron) number density. In Eqs. (11)-(14) the local neutrality condition is assumed, i.e., $n_e(\mathbf{x},0) = n_i(\mathbf{x},0)$, and $\mathbf{E}(\mathbf{x},0) = 0$.

Before solving Eqs. (11)-(15) let us examine the characteristic features for the case where the electron temperature is much less than the ion temperature and the diamagnetic current is wholly carried by the average ion flow. If the plasma is rigidly rotating ($U_i = r\Omega_i$) and the ion pressure P_i is in proportion to $n_i^{\alpha/(\alpha-1)}$ (α is a constant parameter), the solution is written in the form

$$T_i(r,z) = T_0 \left[\Phi(r,z) + \tilde{r}^2/S_*^2 \right], \tag{16}$$

$$n_i(r,z) = n_0 \left[\Phi(r,z) + \tilde{r}^2/S_*^2 \right]^{\alpha-1}, \tag{17}$$

$$P_i(r,z) = P_0 \left[\Phi(r,z) + \tilde{r}^2/S_*^2 \right]^{\alpha}, \tag{18}$$

where

$$\Phi(r,z) = (\Psi_s - \Psi(r,z))/(\Psi_s - \Psi_a), \quad P_0 = n_0 k_B T_0, \quad \tilde{r} = r/r_0,$$

$$S_* = \frac{1}{\sqrt{2\alpha}} \frac{r_0}{\lambda_{i0}} \frac{\Psi_s - \Psi_a}{\pi r_0^2 B_*}, \quad \lambda_{i0} = \frac{v_{Ti}}{\omega_{ci}}, \quad v_{Ti} = \sqrt{k_B T_0/m_i},$$

$$\frac{\Omega_i}{\omega_{ci}} = \frac{1}{S_*^2} \frac{\Psi_s - \Psi_a}{\pi r_0^2 B_*}, \quad \omega_{ci} = \frac{q_i B_*}{m_i c},$$

where $T_i(r,z)$ is the ion temperature, $\Psi(r,z)$ is the poloidal magnetic flux, Ψ_s and Ψ_a are the value at the magnetic separatrix and the value at the field-null point, respectively, T_0, n_0 and P_0 are constant, B_* is the average magnetic field, r_0 is the device radius and k_B is the Boltzmann constant. The second term in the bracket in Eqs. (16)-(18) represents the centrifugal potential which increases in proportion to $1/S_*^2$. The centrifugal potential allows leakage of the plasma beyond the magnetic separatrix ($\Phi = 0$). The parameter $\bar{s}$ is related to S_* as

$$\bar{s} = S_* \frac{\sqrt{\alpha/2}}{\tilde{r}_s} \int_{\tilde{r}_a}^{\tilde{r}_s} \frac{-(d\Phi/d\tilde{r})d\tilde{r}}{[\,\Phi + \tilde{r}^2/S_*^2\,]^{1/2}}, \tag{19}$$

where $\tilde{r}_s = r_s/r_0$ and $\tilde{r}_a = r_a/r_0$. Figure 2 shows the dependences of $\bar{s}$ and Ω_i/ω_{ci} on the parameter S_* for the case where $\alpha = 1.5$ and the separatrix length along the z-axis z_s is equal to $3r_0$. The parameter $\bar{s}$ decreases monotoneously as S_* decreases, and the relation $\bar{s} \approx 1$ holds when $S_* \approx 1$. The normalized angular velocity Ω_i/ω_{ci} increases in proportion to $1/S_*^2$. It is worthy to note that the centrifugal force acting on the ion fluid becomes comparable to the Lorentz force as $\bar{s}$ approaches to 1 (see Eqs. (16)-(18)).

After having obtained a two-fluid equilibrium by solving Eqs. (11)-(15) numerically the position $\mathbf{x}(0)_j$ and the velocity $\mathbf{v}(0)_j$ of the j-th particle are determined from the fluid quantities $P_i(r,z)$, $P_e(r,z)$, $n_i(r,z)$, $n_e(r,z)$, $U_i(r)$ and $U_e(r)$ by using the quiet start technique[14]. We adopt the boundary condition that the physical quantities are periodic at two axial edges of the cylindrical vessel ($z = 0, z_v$; z_v is fixed to $5r_0$ in this paper) and a particle is completely elastically reflected on the conducting wall ($r = r_0$). Both ions and electrons are treated as super-particles which have much larger masses and charges compared with the real masses and charges. The time step Δt is fixed to $2/\omega_{pe}$ where ω_{pe} is the average electron plasma frequency. Numerical scheme used for the three-dimensional particle simulation relies on a semi-implicit method.[12,13] One of the properties of this scheme is that high frequency waves can be artifically damped by introducing a time-decentering technique and hence low frequency phenomena can be described without dropping electron and ion FLR effects.

III. Simulation Results

Four simulation runs with different values of $\bar{s}$ are carried out, where the total number of particles is fixed to 10^5. The simulation runs are terminated after one

Alfven transit time t_A where t_A is defined by r_0/v_A and v_A is the average Alfven velocity. The simulation parameters are listed in Table I. We obtain the initial profiles with different values of $\bar{s}$ by changing the value of the particle mass keeping the fixed mass ratio of $m_i/m_e = 40$.

A. Ion Kinetic Effect on Tilt Stabilization

Before going into consideration of the mechanism of the tilt stabilization, let us start with describing the general feature of the particle motion in the FRC plasma. The initial profiles of the magnetic pressure, the poloidal magnetic field, the ion thermal pressure and the ion mass density in the (r,z)-plane are shown in Fig. 3 for $\bar{s} = 5$, where the radial scale is magnified by two times for convenience. The magnetic pressure has a steep gradient along the r-direction while its value varies moderately along the z-axis. In other words, the magnetic pressure is formed in a fairly prolate shape. The profile of the magnetic field strongly affects the particle behavior. Particularly in the vicinity of the field-null point a particle reveals a fairly complex behavior. As a particle approaches the field-null ponit, the effect of the magnetic field on a particle motion becomes reduced and thus a particle can move more freely. For example, a particle which exists inside the critical point ($x < 2\lambda_i$) takes a relaxed meandering orbit (see Fig. 1). We call this region as the magnetic well for brevity. Then, most of the particles meander without any self-intersection in the magnetic well. The magnetic well has a fairly prolate shape corresponding to the profile of the magnetic pressure, although its width depends on the kinetic energy of each particle. We illustrate the spatial structure of the ratio of the local Larmor radius of the ion with the thermal energy to the scale length of the magnetic field at $t = 0$ in Fig. 4 for the cases of $\bar{s} = 1$ (left) and $\bar{s} = 5$ (right) where the dotted lines show contours less than 0.5 and the solid lines show contours larger than 0.5 (contours larger than 1.0 are not shown for clarity). It is clear from Fig. 4 that the prolate magnetic well is formed in the central plasma region and the area be-

comes wider as $\bar{s}$ decreases.

Figure 5 and Figure 6 show the bird-eye's view (left) and the top view (right) of the orbits of one hundred ions for the cases of $\bar{s} = 1$ (Fig. 5) and $\bar{s} = 5$ (Fig. 6) where each curve represents the ion trajectory during one Alfven transit time from the start of simulation. For the case of $\bar{s} = 5$ the meandering orbit concentrates on a small region near the field-null line. An ion in the outer region moves on a gyration orbit with a relatively small gyroradius. On the other hand, most of the ions move about in the whole plasma region with a large meandering orbit for the case of $\bar{s} = 1$. Thus, the number of particles with a meandering orbit increases as $\bar{s}$ approaches 1. This result indicates that most of the particles exist in the magnetic well for the case of $\bar{s} = 1$ and can move fairly freely without being restrained by the magnetic field. Incidentally, it should be noted that the number of the meandering electrons is much smaller than that of the meandering ions.

With the above preparation in mind let us examine the temporal evolution of the tilt mode by expanding the z-component of the velocity field into the Fourier series. The dependence of the growth rate on the parameter $\bar{s}$ is plotted in Fig. 7, where the growth rate is calculated from the mode ampltitude in the range of $0.4t_A < t < t_A$, the open circle represents the value obtained by the simulation, the vertical line attached to the open circle represents the error bar. The dashed line is drawn to represent the average tendency of the growth rate as a function of $1/\bar{s}$. The growth rate normalized by the MHD value[6] is also listed in the column of γ/γ_{MHD} of Table I. The evolution of the tilt mode is completely suppressed when $\bar{s} \approx 1$. As $\bar{s}$ increases, the tilt mode tends to be more unstable and the growth rate approaches the MHD value. It can be concluded therefore that the stabilization effect due to the finiteness of the ion Larmor radius is very efficient for the FRC tilt mode.

We are now at the position to elucidate the physical mechanism of the ion kinetic effect on tilt stabilization. In doing so let us first consider the tilting instabili-

ty for the MHD case. Suppose that a perturbation of $n = 1$ tilt mode is added to the initial two-dimensional equilibrium. The perturbation gives rise to the $n = 1$ modification of the plasma current profile. A torque force is then generated by the vector product between the perturbed plasma current and the external field, whereby the tilt modification is accelerated. This comes from the fact that the MHD plasma is frozen in the magnetic field. On the other hand, for the kinetic plasma of $\bar{s} = 1$ most of the ions are free from the constraint of the magnetic field and oscillate around the field-null point with a large amplitude, as was shown in Fig. 5. Suppose that the direction of the velocity of the tilting perturbation is in phase with that of the meandering oscillation of an ion. Then, the ion changes to a new oscillation orbit with a larger amplitude, but with the same oscillation center. When the direction of the perturbed velocity is opposite, the ion executes a smaller amplitude oscillation, but the oscillation center remains the same in this case, as well. When the orbit is averaged over one oscillation period for either case, therefore, the toroidal current carried by the meandering ion does not contribute to the $n = 1$ tilt modification of the plasma current profile in the average. In other words, the ion with a meandering orbit does not contribute to the growth of the perturbation of the $n = 1$ tilt mode. We thus conclude that the ion with a meandering orbit plays a key role in keeping the system stable against the tilting instability, and that the evolution of tilt mode can be completely suppressed when most of the ions move on the stable meandering orbits, i.e., when $\bar{s} \approx 1$. In this respect note that the drift direction of the meandering ions is the same as the direction of the ion diamagnetic current, though the gradient-B drift is opposite (see, Fig. 1), this supporting the above argument that the meandering ions contributing to the toroidal current plays a vital role in tilt stabilization.

B. Anisotropy of Pressure Profile

The profiles of the ion distribution and the electron distribution in the velocity

space are shown in Fig. 8 (ion) and Fig. 9 (electron) for the case of $\bar{s} = 2$, where the top panels show the initial distributions in the (v_r, v_z)-plane (left) and in the (v_ϕ, v_z)-plane (right), and the bottom two panels show the distributions at $t = t_A$. The dashed lines represent the coordinate axes and the dotted line represents the average value of the toroidal velocity $<v_\phi>$. The ion distribution which is isotropic at $t = 0$ changes to the distribution with an anisotropic temperature of $T_z > T_r, T_\phi$ after one Alfven transit time, while the electron distribution remains almost isotropic during the simulation run.

This phenomenon can be easily explained by the anisotropic meandering orbit. As was mentioned before, the prolate magnetic well with a steep wall along the r-direction is formed in the FRC plasma. A particle that can execute an oscillation in the z-direction has a smaller energy compared with a particle that can execute an oscillation in the r-direction, because the scale height x_0 in the z-direction is larger than that in the r-direction. (Note that the characteristic value of magnetic field B_0 varies in proportion to $1 / x_0^2$ if the poloidal magnetic flux inside the radius x_0 is conserved.) Accordingly, the particles with the z-oscillation predominantly exist in the prolate magnetic well and the ion distribution with an anisotropic temperature of $T_z > T_r$ is realized in the FRC plasma.

Since the pressure anisotropy is deeply connected with the number of meandering particles, it is expected that the pressure profile approaches an isotropic one as the number of meandering particles decreases. The last two columns of Table I show the ion pressure anisotropy P_{zi} / P_{ri} and the electron pressure anisotropy P_{ze} / P_{re} at the plasma center for the runs with four different values of $\bar{s}$. As can be clearly seen, the ion anisotropy is roughly inversely proportional to $\bar{s}$ while the electron distribution keeps almost isotropic regardless of $\bar{s}$. Thus we can conclude that the pressure anisotropy is caused by the anisotropy of the meandering orbit.

C. Plasma Rotation

Finally, we shall examine the structure of the average toroidal (ϕ) flow. We can find in Fig. 8 that only the high energy ions shift in the positive ϕ-direction at $t = t_A$ in spite of the fact that all the components have had the positive toroidal shift at $t = 0$. This means that the greater part of the toroidal ion (positive ϕ) current is carried by the meandering ions. In this respect one should note that the drift direction of the meandering ions is reversed in comparison with that of the gradient-B drift when $\lambda_i/x_0 > 0.303$, more specifically, the drift direction of the meandering ions becomes the same as the direction of the toroidal current, thus positively contributing to the toroidal current.

Figure 10 shows the temporal evolutions of the Mach numbers of the ion toroidal flow (possitive) and the electron toroidal flow (negative) for the runs with four different values of $\bar{s}$, where the Mach number is calculated at the field-null point. The Mach number of the electron flow is plotted in the negative region of Fig. 10 because the average electron flow always directs in the negative ϕ-direction. The nature that the average velocity of the electron toroidal flow is always negative is attributed to the electron diamagnetic drift. The Mach number of the ion toroidal flow changes approximately inversely proportional to the value of $\bar{s}$ and the rotational velocity of the ion flow reaches the value a little larger than half of the thermal velocity for the case of $\bar{s} = 1$. If the orbit motion is averaged over one oscillation period, the meandering orbit with no self-intersection has a larger average toroidal velocity than the drift orbit with self-intersection (see Fig. 1). Therefore, the average fluid velocity along the field-null line increases as the parameter $\bar{s}$ decreases, that is, the number of the meandering particles increases. It should be noted that the rotation speed obtained here is much smaller than the threshold value for the spin stabilization evaluated by using the MHD simulation,[6,15] thus indicating that the stabilization effect observed in our simulation study is not due to the spin effect.

The spatial structure of the ion toroidal flow velocity is shown in Fig. 11 for the case of $\bar{s} = 3$, where the top perspective diagram represents the initial structure

in the (r,z)-plane and the bottom diagram represents the final structure. The rigid rotor is assumed in the initial equilibrium profile. As time elapses, the initial profile is modified and the high speed component appears near the top and bottom edges where the field lines are sharply curved. By examining the property of the magnetic curvature drift in the final profile it is found that both the spatial structure and the amplitude of the magnetic curvature drift are in good agreement with those of the modified ones. As the number of the meandering ions increases, the difference from the rigid rotor is reduced. We here note that the development of the $n = 2$ rotational instability is not observed for any cases in one Alfven transit time.

IV. Summary and Discussions

In order to investigate the ion kinetic stabilization effect on the tilting instability in the FRC plasma we have developed a three-dimensional particle simulation code which can describe both the microscale particle motions and the magnetohydrodynamic evolutions in the cylindrical coordinates. By carrying out four simulation runs with different values of $\bar{s}$ we have been able to clarify the role of the ion kinetic effects on the stabilization of the FRC tilt disruption. The main results can be summarized as follows.

(A) The growth rate of the tilting instability decreases as the parameter $\bar{s}$ decreases and the instability is completely suppressed when $\bar{s} \approx 1$. This kinetic stabilization effect is attributed to the characteristics of the ions which execute meandering motions around the field-null line. The meandering ion orbit shifts to the orbit with a little larger/smaller oscillation amplitude, however, the average behavior of the meandering ions does not contribute to the tilt modification of the plasma current because of their oscillatory motion around the same oscillation center. As $\bar{s}$ becomes smaller, the number of the meandering ions increases and thus the ion kinetic stabilization becomes more efficient.

(B) The meandering ion preferably oscillates along the z-direction because of

the exisitence of the prolate magnetic well with the steep magnetic wall along the r-direction. The anisotropy of the meandering orbit results in the anisotropy of the ion pressure profile. The degree of the anisotropy decreases as the number of the meandering ions decreases.

(C) The toroidal ion current is mainly carried by the meandering ions with high energy. The ion toroidal flow velocity increases as $\bar{s}$ decreases and the Mach number is nearly equal to 0.5 for the case of $\bar{s} = 1$. The spatial profile of the plasma rotation is modified by the magnetic curvature drift at the sharply curved edges of field lines. The modification becomes smaller as the number of meandering ions increases.

Let us briefly touch on the role of the electric field on the tilt stabilization. We have obtained the initial equilibrium by assuming that the electric field would not play an essential role in the global instability, such as the tilt mode. The temporal evolutions of the electric field energy in the present study are shown in Fig. 12 for four different $\bar{s}$ cases. Here, the electric field is expressed in such a normalized unit that the average magnetic field is nearly equal to 1. It is clear in Fig. 12 that the electric field remains at a considerably low level compared with the magnetic field for four cases, though the values slowly change in time and have the $\bar{s}$-dependence. Thus, we can conclude that the electric field cannot play an essential role in the stability of the tilt disruption.

Before concluding this paper let us discuss the applicability of the model developed here. In general the numerical error appears in the form of the thermal noise due to the finiteness of the number of the particles used in the simulation. In this paper we dealt with a hundred thousand particles. The number of the particles in a cell is around twenty at the central region of the FRC plasma while there are only a few particles in a cell near the plasma boundary. Therefore, a numerical noise tends to be created at the boundary of the FRC plasma. In order to reduce the numerical effect from the simulation we used a low-pass-filter.[6] As a result the fluc-

tuation level of the numerical noise is kept always less than 10 % of the tilt mode. As far as the tilting instability is concerned, the influence of the numerical noise is therefore not predominant. If one wishes to investigate the phenomenon in the edge region, the simulation with much more particles will be needed.

We have obtained the initial condition by solving the two-fuild MHD equilibrium. As $\bar{s}$ approaches 1, the discrepacy between the MHD equilibrium state and the particle equilibrium state appears because of the ion finite Larmor radius effect. In order to exclude the influence of this discrepacy from the simulation results the analysis of the tilt mode is carried out after the plasma configuration is relaxed to a quasi-equilibrium state in the simulation ($t > 0.4t_A$). An alternative way is to solve the Maxwell-Vlasov equations and start the simulation from the solution. However, it is fairly difficult to solve the two-dimesional Maxwell-Vlasov equations in the cylindrical coordinates because of the highly nonlinear nature. We hope that these problems will be solved elsewhere.

Acknowledgments

We are grateful to Prof. K. Nishikawa for his continuous interest in this work and Dr. M. Tanaka for his kindness in using his semi-implicit particle simulation scheme. This work is supported by a Grant-in-Aid for Fusion Research from the Japanese Ministry of Education, Science and Culture.

References

[1] S. Ohi, T. Minato, Y. Kawakami, M. Tanjyo, S. Okada, Y. Ito, M. Kako, S. Goto, T. Ishmura, and H. Ito, Phys. Rev. Lett. **51**, 1042(1983): A. L. Hoffman, J. T. Slough, and D. G. Harding, Phys. Fluids **26**, 1626(1983).

[2] W. N. Rosenbluth, M. N. Bussac, Nucl. Fusion **19**, 489(1979): J. H. Hammer, Nucl. Fusion **21**, 488(1981).

[3] J. L. Schwarzmeier, D. C. Barnes, D. W. Hewett, C. E. Seyler, A. I. shestakov, and R. L. Spencer, Phys. Fluids **26**, 1295(1983).

[4] R. A. Clemente and C. E. Grillo, Phys. Fluids **27**, 658(1984).

[5] For example, A. G. Eskov, R. Kh. Kurtmullaev, A. P. Kreshchuk, Ya. N. Laukhin, A. I. Malyutin, A. I. Markin, Yu. S. Martyushov, B. N. Mironov, M. M. Orlov, A. P. Proshletsov, V. N. Semenov, and Yu. B. Sosunov, in *Plasma Physics* and *Controlled Nuclear Fusion Research* (IAEA,Vienna,1979), Vol. 2, p.187: W. T. Armstrong, D. G. Harding, E. A. Crawford, and A. L. Hoffman, Phys. Fluids **25**, 2121(1982).

[6] R. Horiuchi and T. Sato, Phys. Fluids **B1**, 581(1989).

[7] D. C. Barnes, J. L. Schwarzmeier, H. R. Lewis, and C. E. Seyler, Phys. Fluids **29**, 2616(1986).

[8] A. Ishida, H. Momota, and L. C. Steinhauer, Phys. Fluids **31**, 3024(1988).

[9] R. D. Milroy, D. C. Barnes, R. C. Bishop, and R. B. Webster, Phys. Fluids **B1**, 1225(1988).

[10] J. T. Slough, A. L. Hoffman, Nucl. Fusion **28**, 1121(1988).

[11] J. S. Kim and J. R. Cary, Phys. Fluids **26**, 2167(1983).

[12] M. Tanaka and T. Sato, Phys. Fluids **29**, 3823(1986).

[13] M. Tanaka, T. Sato and A. Hasegawa, Phys. Fluids **B1**, 325(1989).

[14] C. K. Birdsall and A. B. Langdon, in *Plasma Physics Via Computer Simulation* (Mcgraw-Hill Book Company, New York, 1985).

[15] R. D. Milroy, D. C. Barnes, R. C. Bishop, and D. D. Schnack, in *Proceedings of the 12th conference on the numerical simulation of plasmas* (San Francisco, 1987).

Table I. Simulation parameters

$\bar{s}$	m_i/m	m_e/m	q_i/e	v_{Ti}/c	λ_{i0}/r_0	γ/γ_{MHD}	P_{zi}/P_{ri}	P_{ze}/P_{re}
1.0	$1.0\cdot10^{6}$	$2.5\cdot10^{4}$	$1.0\cdot10^{5}$	$1.9\cdot10^{-2}$	$1.9\cdot10^{-1}$	0.01	1.71	1.02
2.0	$4.8\cdot10^{5}$	$1.2\cdot10^{4}$	$1.0\cdot10^{5}$	$2.0\cdot10^{-2}$	$9.5\cdot10^{-2}$	0.05	1.57	0.96
3.0	$3.2\cdot10^{5}$	$8.0\cdot10^{3}$	$1.0\cdot10^{5}$	$2.0\cdot10^{-2}$	$6.3\cdot10^{-2}$	0.24	1.40	1.04
5.0	$2.0\cdot10^{5}$	$5.0\cdot10^{3}$	$1.0\cdot10^{5}$	$1.9\cdot10^{-2}$	$3.8\cdot10^{-2}$	0.38	1.29	1.03

Table caption

Table I Simulation parameters. The column of γ/γ_{MHD} shows the growth rate γ nomalized by the MHD value γ_{MHD} for $0.4t_A < t < t_A$ and the last two columns represent the anisotropies of the ion and electron pressures at $t = t_A$. The electron charge q_e used in the simulation is equal to $-q_i$. The parameters m ($= 9.1\cdot10^{-28} gr$) and e ($= 4.8\cdot10^{-10} esu$) are the real mass and the real charge of an electron, respectively.

Figure captions

Fig. 1 Eight types of ion orbit in the one-dimensional neutral sheet model. The magnetic field has only the z-component and its value depends only on the coordinate x in the form as $B_z(x) = B_0(x/x_0)$, where x_0 is the scale hight and B_0 is the characteristic value of magnetic field. The solid curve shows the ion trajectory which starts with a negative velocity $-v_y$ from the point $(x_0,0)$. The Larmor radius λ_i at the starting point is given by $v_y/(q_iB_0/m_ic)$ with a particle mass m_i and a particle charge q_i.

Fig. 2 The dependence of $\bar{s}$ and Ω_i/ω_{ci} on the parameter S_* in the cold electron model. The profile parameter α is assumed to be 1.5 and the separatrix length along the z-axis z_s is fixed to $3r_0$. The scale on the left vertical axis measures Ω_i/ω_{ci} and the scale on the right vertical axis measures $\bar{s}$.

Fig. 3 The initial profiles of the magnetic pressure $B^2/2$, the poloidal magnetic field, the ion thermal pressure P, and the ion mass density ρ in the (r,z)-plane for the case of $\bar{s} = 5$, where the radial scale is magnified by two times for convenience. The small bottom panel shows the radial distribution in the mid-plane of the upper panel.

Fig. 4 The initial profiles of the ratio of the local ion Larmor radius to the scale length of the magnetic field for the cases of $\bar{s} = 1$ (left) and $\bar{s} = 5$ (right), where the radial scale is magnified by two times for convenience. The dotted lines show contours less than 0.5 and the solid lines show contours larger than 0.5 (contours larger than 1.0 are not shown for clarity).

Fig. 5 The bird-eye's view (left) and the top view (right) of the orbits of one

hundred ions for the case of $\bar{s} = 1$. Each curve represents the ion trajectory during one Alfven transit time from the start of simulation and a closed circle attached to each curve show the starting point.

Fig. 6 The same figure as Fig. 5 for the case of $\bar{s} = 5$.

Fig. 7 The $\bar{s}$-dependence of the growth rate of the tilting instability. The open circle represents the value obtained by the simulation, and the vertical line attached to the open circle represents the error bar. The dashed line represents the average tendency of the growth rate as a fucntion $1 / \bar{s}$.

Fig. 8 The ion distribution in the velocity space for the case of $\bar{s} = 2$. The top panels show the initial distributions in the (v_r, v_z)-plane (left) and in the (v_ϕ, v_z)-plane (right), and the bottom two panels show the distributions at $t = t_A$. The dashed lines show the coordinate axes and the dotted line shows the average value of the ion toroidal velocity $<v_\phi>$.

Fig. 9 The electron distribution in the velocity space for the same case as Fig. 8. The top panels show the initial distributions in the (v_r, v_z)-plane (left) and in the (v_ϕ, v_z)-plane (right), and the bottom two panels show the distributions at $t = t_A$. The dashed lines show the coordinate axes and the dotted line shows the average value of the electron toroidal velocity $<v_\phi>$.

Fig. 10 The time histories of the Mach numbers of the ion toroidal flow (possitive) and the electron toroidal flow (negative) for the cases where $\bar{s}$ is equal to 1, 2, 3 and 5, respectively. The Mach number is calculated at the field-null point. The Mach number of the electron flow is plotted in the negative region because the average toroidal electron velocity is always

negative.

Fig. 11 The perspective diagrams of the ion toroidal flow velocity at $t = 0$ (top) and $t = t_A$(bottom) for the case of $\bar{s} = 3$. Here, the vertical axis shows the toroidal velocity in the (r,z)-plane which is averaged in terms of the ϕ-variation.

Fig. 12 The time histories of the electric field energy for the same cases as Fig. 10 where the electric field is obtained in a normalized unit.

Fig. 1

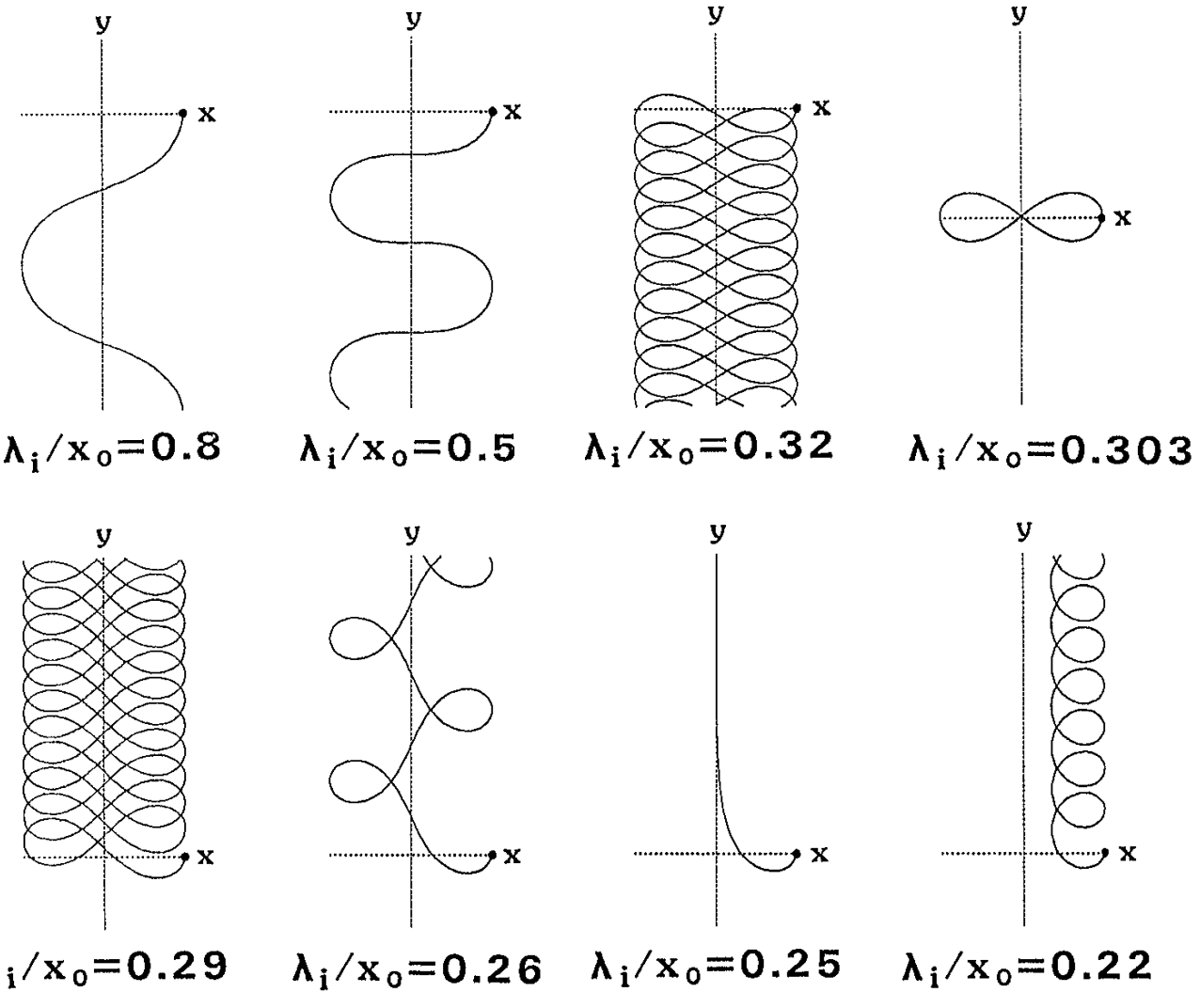
y
x
$\lambda_i/x_o=0.8$
$\lambda_i/x_o=0.5$
$\lambda_i/x_o=0.32$
$\lambda_i/x_o=0.303$
$\lambda_i/x_o=0.29$
$\lambda_i/x_o=0.26$
$\lambda_i/x_o=0.25$
$\lambda_i/x_o=0.22$

Fig. 2

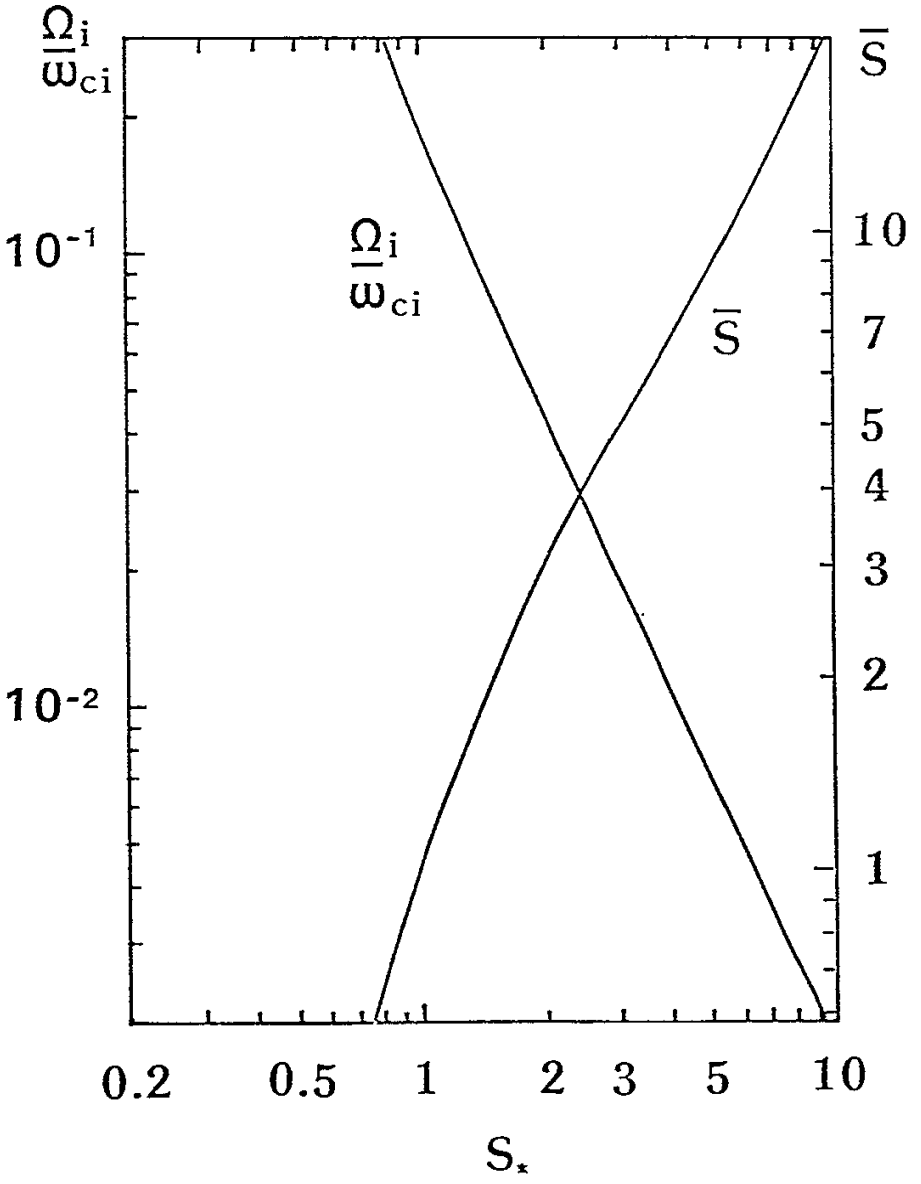

Fig. 3

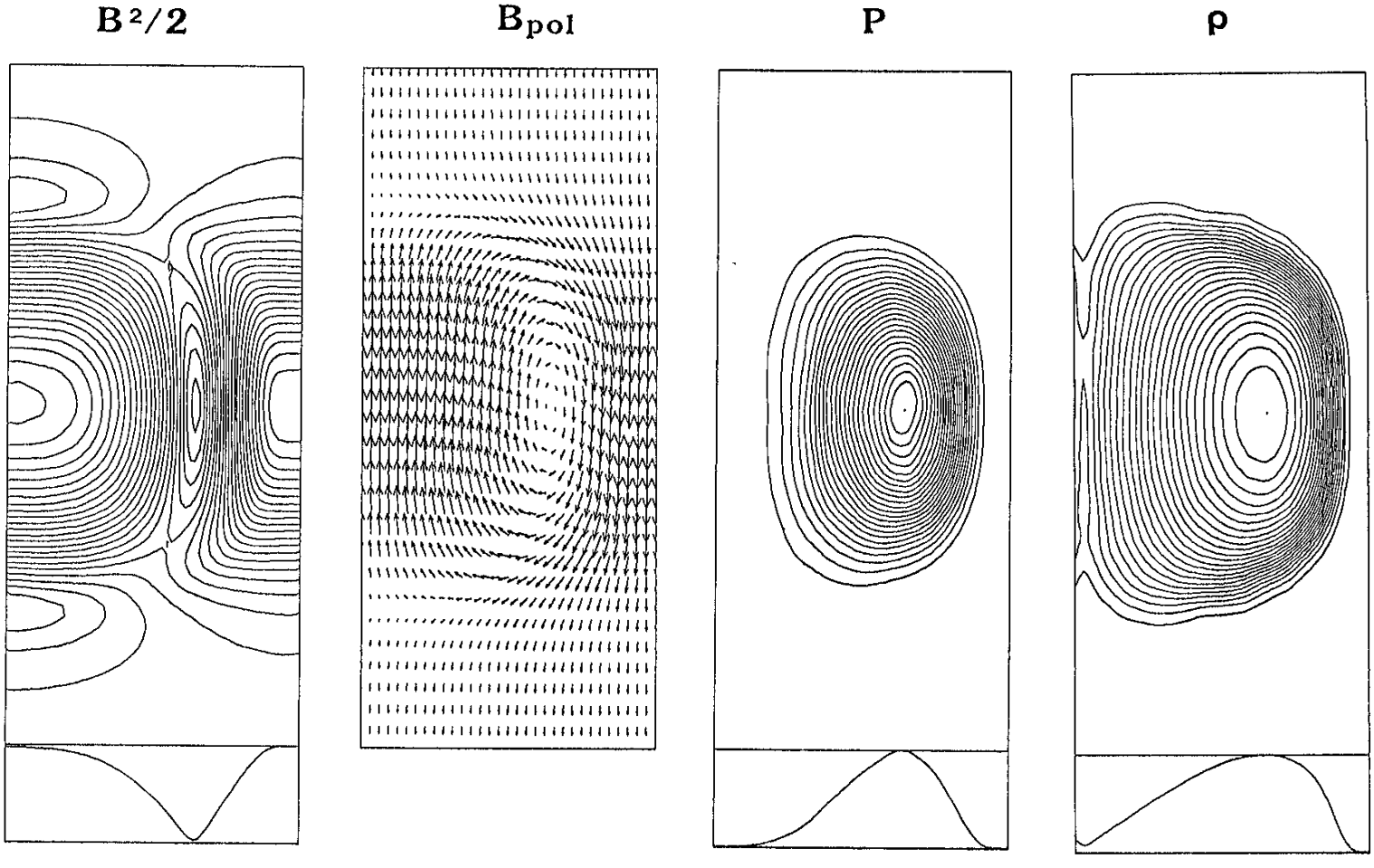

Fig. 4

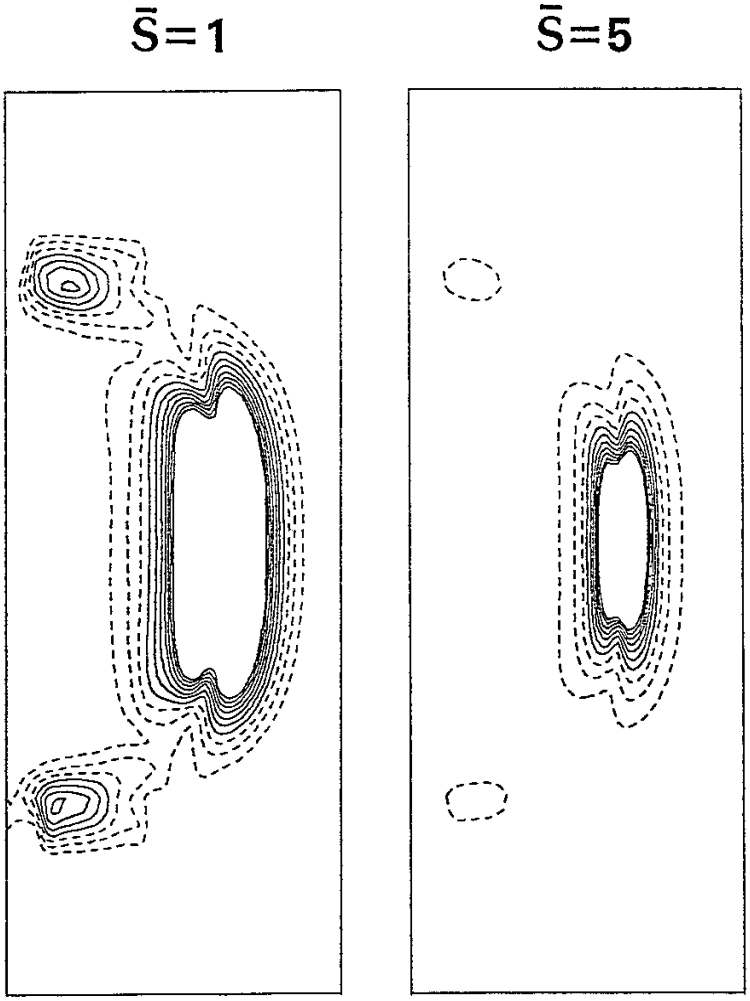

Fig. 5

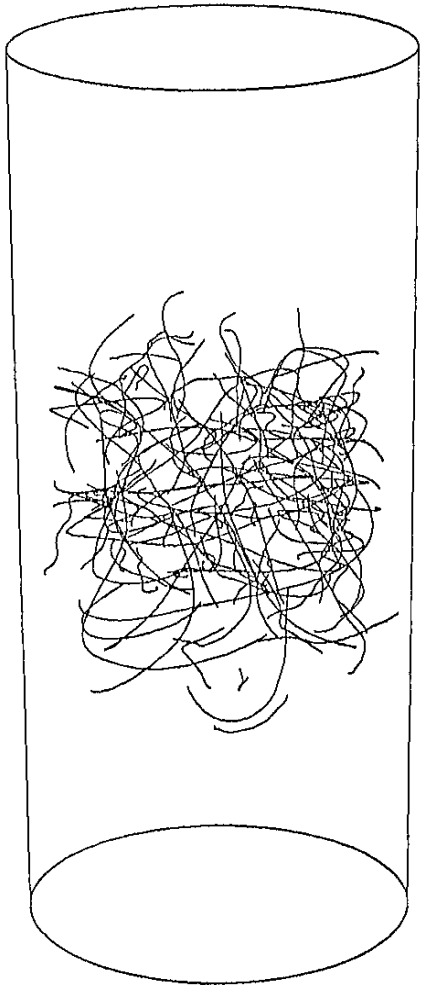

$\overline{S}=1$

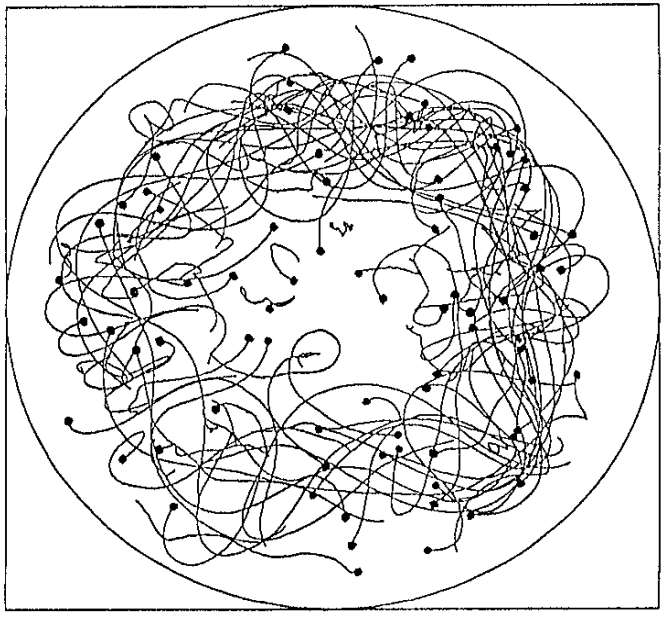

Fig. 6

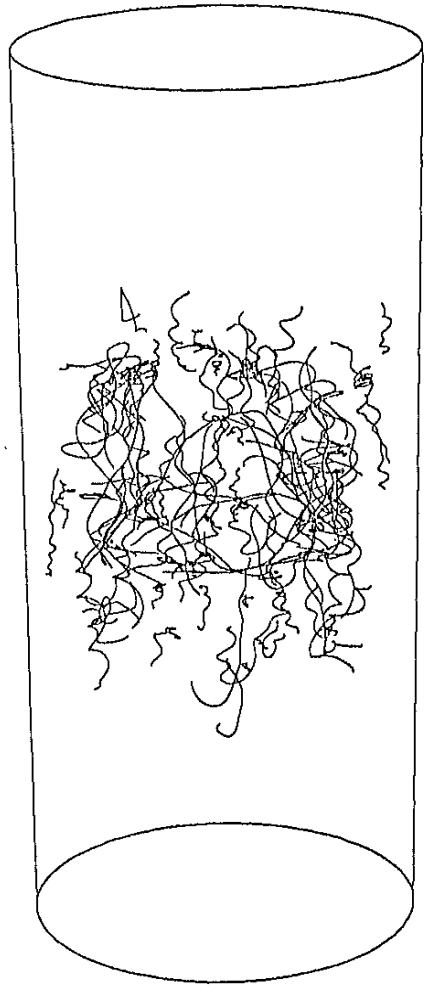

$\bar{S}=5$

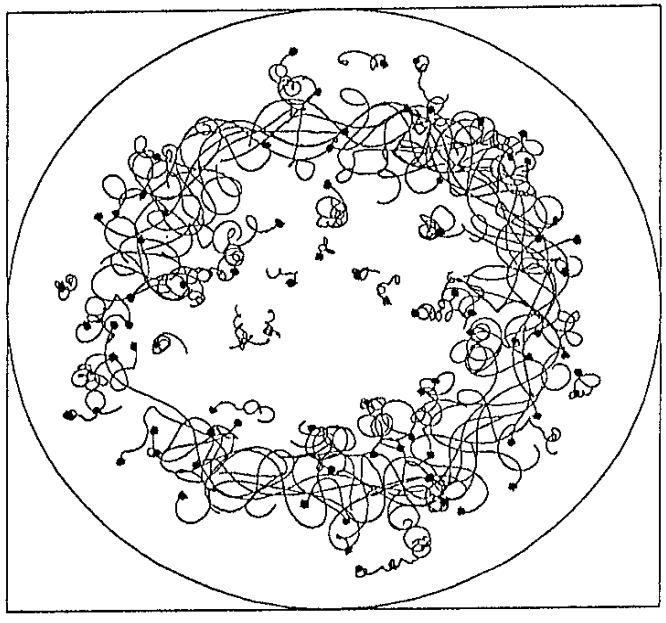

Fig. 7

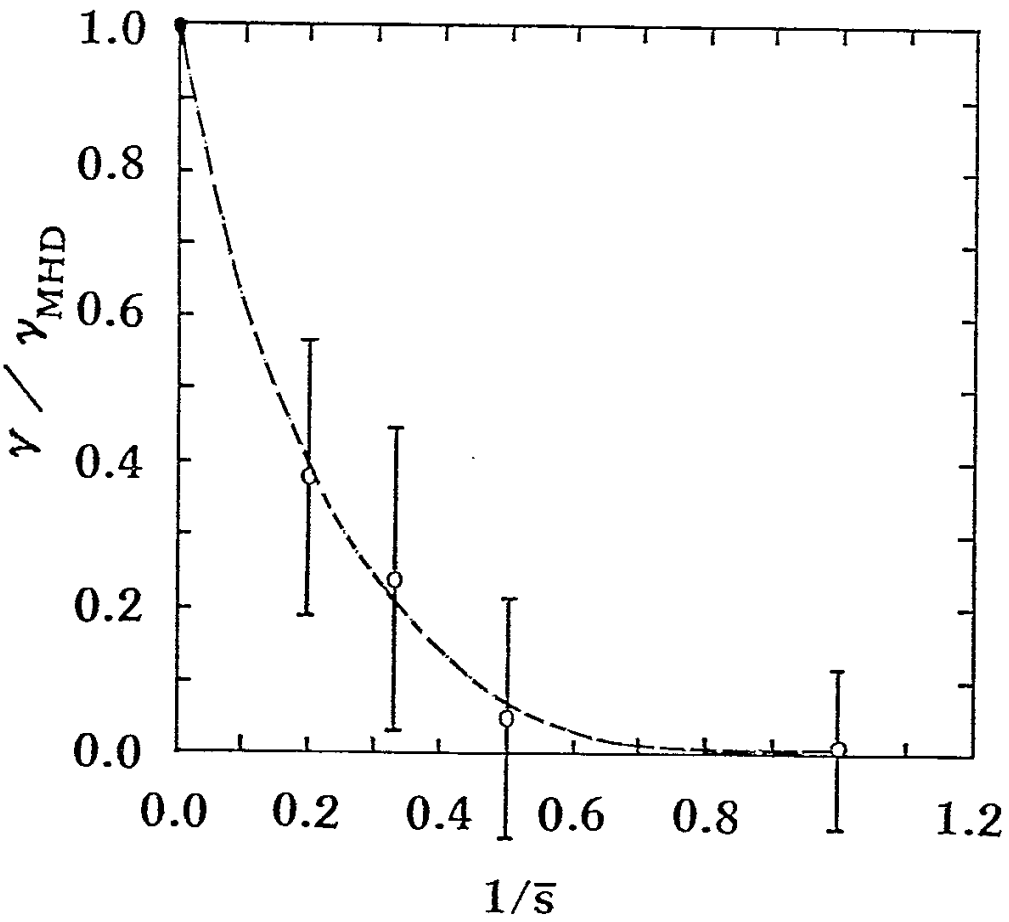

Fig. 8

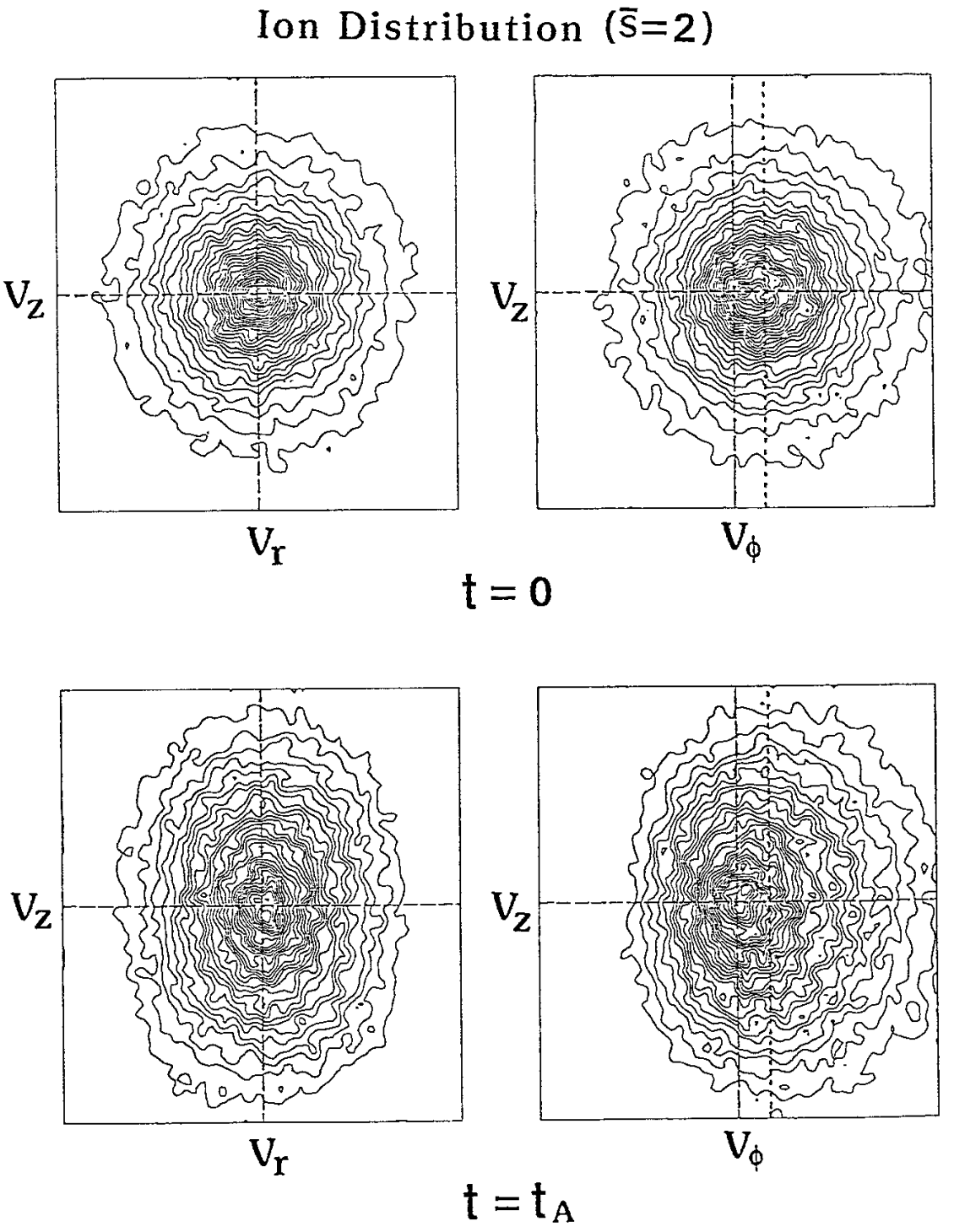

Fig. 9

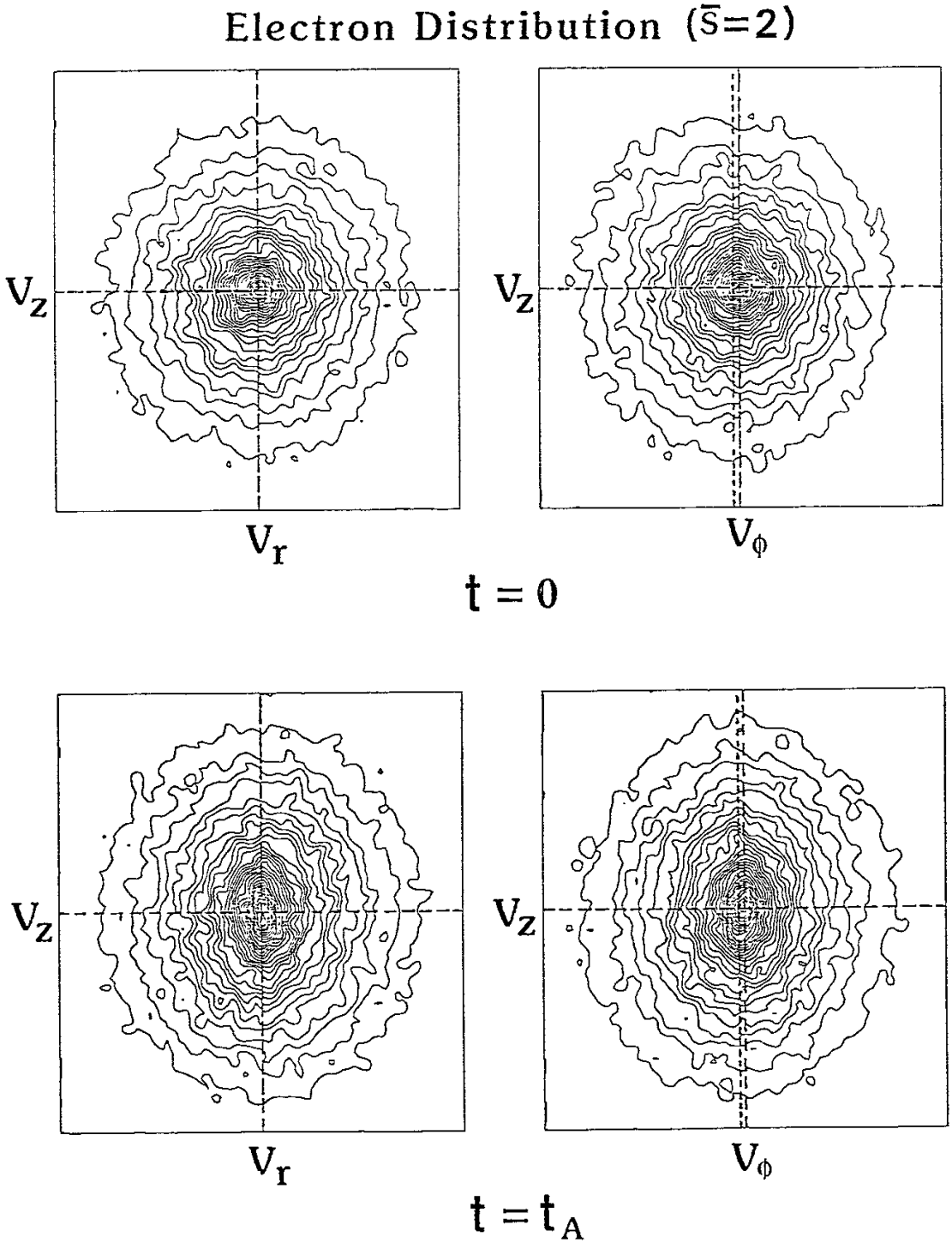
Electron Distribution ($\bar{s}$=2)
V_z
V_r
V_z
V_ϕ
t = 0
V_z
V_r
V_z
V_ϕ
$t = t_A$

Fig. 10

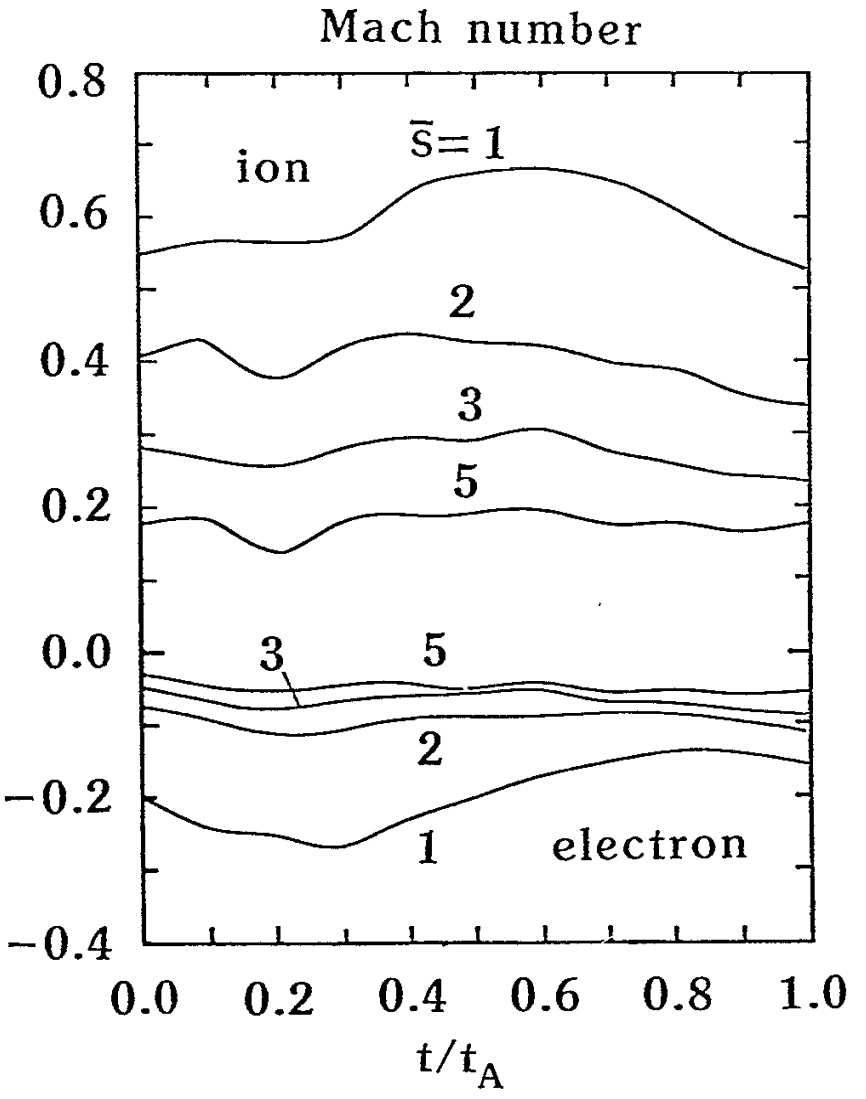
Mach number
0.8
0.6
0.4
0.2
0.0
−0.2
−0.4
ion
$\bar{S}$= 1
2
3
5
3
5
2
1
electron
0.0
0.2
0.4
0.6
0.8
1.0
t/t$_A$

Fig. 11

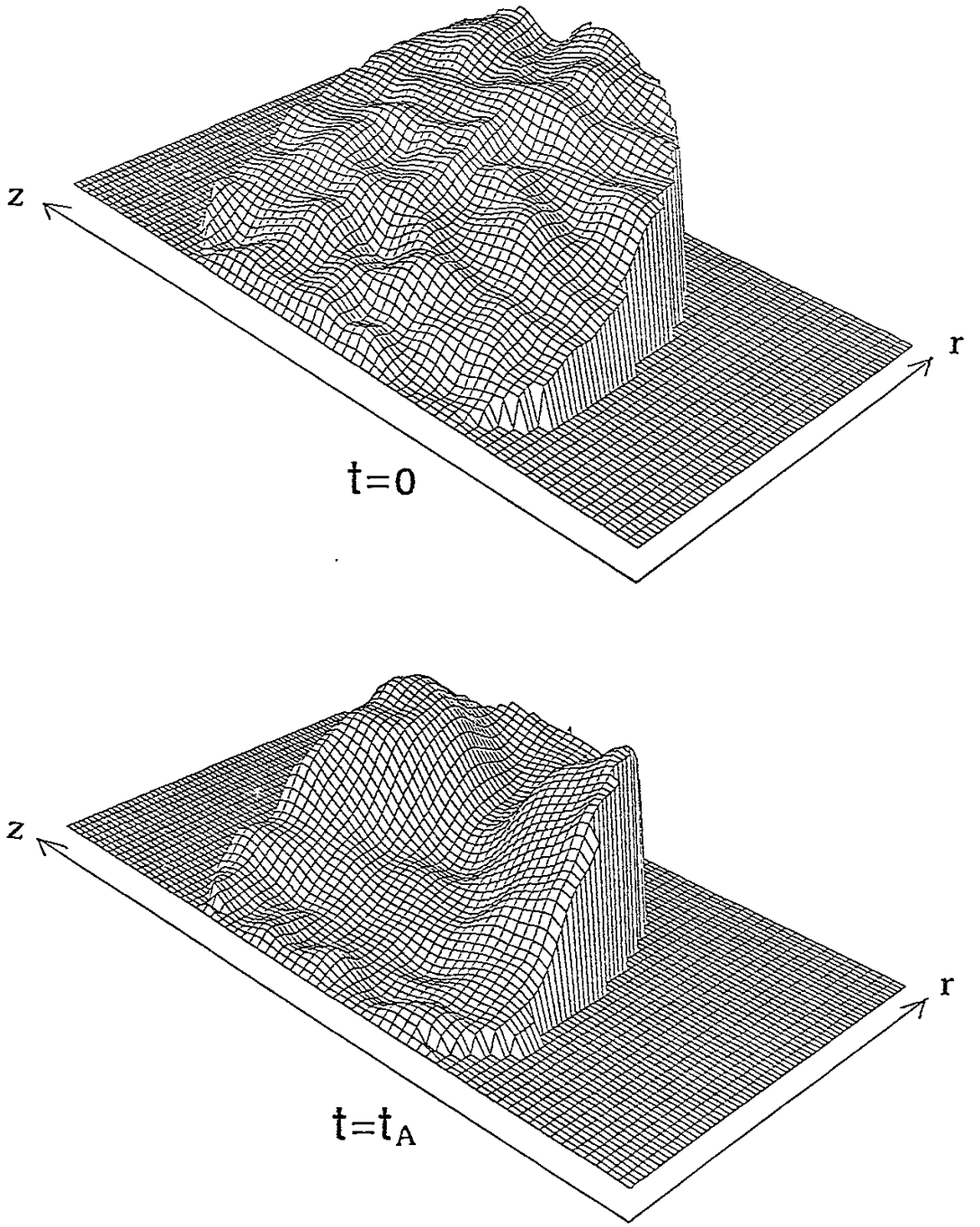

Fig. 12

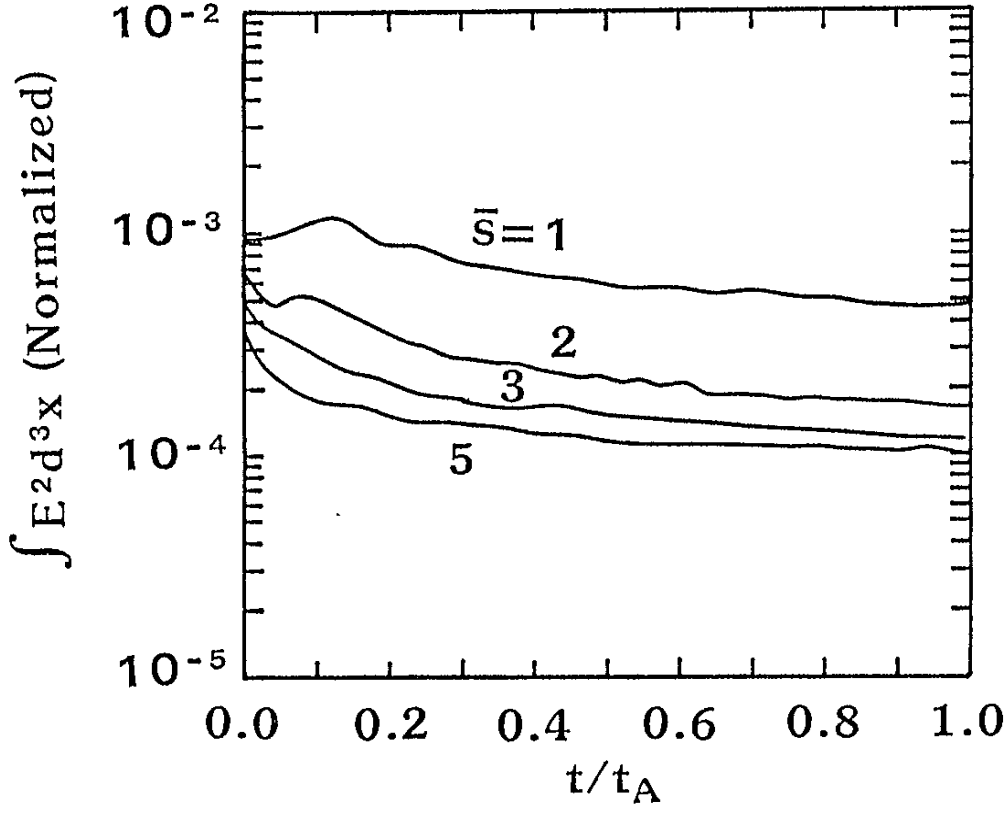
10^{-2}
10^{-3}
10^{-4}
10^{-5}
$\int E^2 d^3x$ (Normalized)
$\bar{S}=1$
2
3
5
0.0
0.2
0.4
0.6
0.8
1.0
t/t_A